Cent. Eur. J. Phys. • 11(9) • 2013 • 1082-1090
DOI: 10.2478/s11534-013-0232-2

VERSITA

Central European Journal of **Physics**

A rate equation method for the sequential double ionisation, including autoionising state excitation, of a noble gas

Research Article

Damien P. W. Middleton[1,2*], Katravulapally N. R. Tejaswi[1,2], Lampros A. A. Nikolopoulos[1,2]

1 *School of Physical Sciences, Dublin City University, Collins Ave., Dublin 9, Dublin, Ireland*

2 *National Centre for Plasma Science & Technology, Dublin City University, Collins Ave., Dublin 9, Dublin, Ireland*

Received 29 December 2012; accepted 10 April 2013

Abstract: A set of rate equations have been tested against a more robust set of Time-Dependent Density Matrix (TDDM) equations [D. P. W. Middleton, L. A. A. Nikolopoulos, J. Mod. Opti. 59, 1650 (2012)] by using them to determine the populations of ion species and autoionising states (AIS) in noble gas atoms when interacting with a strong external field. Two field shapes were tested here - sinusoidal and square - and a variety of pulse characteristics were examined, i.e. intensity, duration and photon energy, for the neon atomic system. It was found that the rate equations were sufficiently accurate only when the external field is way off-resonant with the AIS. Moreover, analytical solutions of the rate equations in the square pulse case agree with the numerical solutions for a time-dependent pulse containing many cycles. An attempt to model a stochastic field was also made and it was found that the use of such a field diminished and broadened the ion yield ratio due to the presence of an added bandwidth.

Keywords: noble gas • autoionising state • neon • rate equation • analytical equation

1. Introduction

A rate equation approach to solving generic atomic systems under the influence of strong UV/X-ray laser fields is a powerful tool. Since these laser fields have become available to experimenters, through the use of free-electron lasers (FEL) such as LCLS, FLASH, [1–3] etc., the theoretical community has been working to advance theoretical and computational methods in order to test the results obtained through experiment [2–5]. To date, there is no time-dependent theory that can treat double ionisation of noble gas atoms in their full dimensionality. Also, the presence of a strong resonance with an AIS adds to the complexity of the problem. However, other methods, such as time-dependent density matrix (TDDM) methods [6–10], have proven to be useful. These methods can also be further simplified, resulting in the so-called rate equation approach. Thus, a simple computational approach may be derived from a more complicated application, which can then be used to model systems of noble gases and their ionisation dynamics, $A \rightarrow A^{+} \rightarrow A^{2+}$, under these conditions. Furthermore, when using approximations for the pulse shape, an analytical solution may be derived [11],

*E-mail: damien.middleton3@mail.dcu.ie

which can be used to quickly determine an approximation to the results one might expect from an experiment.

In the present work we have used a rate equation approach for such systems and tested its applicability against a more complete TDDM method [6]. We have calculated the populations of the ionic states under different pulse conditions such as intensity, duration, photon energy and shape, and have compared the results to those obtained using the TDDM approach. We have also calculated the populations using a set of analytical equations under simplified pulse conditions and have compared these results with the rate equation results in order to determine their validity.

In Section 2, a brief description of the method of derivation and of the equations used is given. In Section 3, the results of the ionisation dynamics involving AIS resonances and under different pulse conditions, are presented and discussed. Finally, conclusions are made in Section 4 about the applicability of the rate and analytical equations.

2. The theoretical framework

A restricted subspace of the full problem is used such that only those states that are expected to be most relevant to the problem under consideration are included. The particular choice of the subspace depends on the atomic system itself and the experimental conditions one wants to model. The system begins in the neutral noble gas atom state, represented by $|g\rangle$, and an intense pulse is switched on smoothly at this point. The energy of this state is E_g and we say that at $t = 0$, the population of this state is equal to one. That is to say that the population of the system is entirely in the neutral state when the pulse is switched on. The atom can undergo a photo-ionisation process whereby it becomes singly ionised to the intermediate state $|i\rangle$, which represents the ionic state. The energy of this state is given by E_i.

From here, two different absorption processes can occur. Ionisation into the doubly ionised continuum is described through the Fano formulation [12] where $|a\rangle$ represents the bound AIS part with an energy E_a. $|f\rangle$ represents the continuum part of the physical continuum state with energy E_f. From the AIS, there are also two processes that can occur. A Rabi oscillation can occur due to the presence of the field, thus de-exciting the AIS back to the intermediate state, or the AIS can decay via a field-independent coupling to the second continuum. These states and their absorption and decay processes are depicted in Fig. 1.

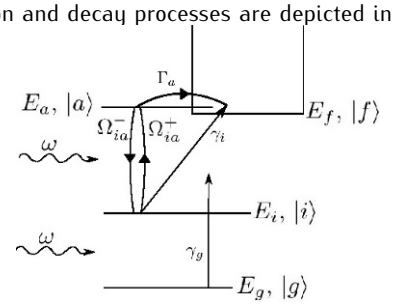

Figure 1. The states involved in the transitions for the noble gas system. The terms in this figure are described in Sections 2 and 2.1.

2.1. The rate equations

A brief description of the equations is given here in order to define any approximations made by the derivation procedure, which has been detailed elsewhere [6]. Using our definition of the system, a set of TDDM equations are derived by substituting the restricted subspace in place of the wavefunction into the Liouville equation [10] and using the rotating wave approximation and the slowly varying approximation. These TDDM equations are demanding to solve computationally. However, by adiabatically eliminating the coherence equations from the TDDM equations, one is left with a set of rate equations. The TDDM equations and the validity of the adiabatic elimination process is discussed elsewhere [6, 7, 13] and so, we have not detailed the procedure here. Starting with the TDDM equations derived in [6], the rate equations are derived. In the case were one intermediate state and one AIS are used, these equations are:

$$\dot{\sigma}_{gg}(t) = -\gamma_g \sigma_{gg}, \tag{1a}$$

$$\dot{\sigma}_{ii}(t) = \gamma_g \sigma_{gg} - \left(\gamma_i + \Omega_{ia}^- + \frac{|\Omega_0|^2}{q_a}\frac{\Delta E_{ai}}{\Delta E_{ai}^2 + [(\gamma_i + \Gamma_a)/2]^2}\right)\sigma_{ii} + \Omega_{ia}^+ \sigma_{aa}, \tag{1b}$$

$$\dot{\sigma}_{aa}(t) = \Omega_{ia}^+ \sigma_{ii} - \left(\Gamma_a + \Omega_{ia}^- + \frac{|\Omega_0|^2}{q_a}\frac{\Delta E_{ai}}{\Delta E_{ai}^2 + [(\gamma_i + \Gamma_a)/2]^2}\right)\sigma_{aa}, \tag{1c}$$

$$\sigma_{ff}(t) = 1 - \sigma_{gg}(t) - \sigma_{ii}(t) - \sigma_{aa}(t), \tag{1d}$$

where

$$\Omega_{ia}^{\pm} = \frac{|\Omega_0|^2}{2}\left(\frac{(\gamma_i+\Gamma_a)/2}{\Delta E_{ai}^2+[(\gamma_i+\Gamma_a)/2]^2}\right)\left(1\pm\frac{1}{q_a^2}\right) \quad (2)$$

is the effective Rabi frequency between the two bound states $|i\rangle$ and $|a\rangle$ and $\Omega_0(t) = \mu_{ia}\mathscr{E}_0(t)$, where μ_{ia} is the dipole transition element for the bound-bound transition $|i\rangle \rightarrow |a\rangle$. $\Delta E_{ai}(t) = \bar{E}_a(t) - (\bar{E}_i(t) - \omega)$ is the detuning of the laser field where $\bar{E}_a(t) = E_a + S_a(t)$ and $\bar{E}_i(t) = E_i + S_i(t)$ include the Stark shifts $S_a(t)$ and $S_i(t)$ of the states due to their interaction with the field. However, the Stark shifts are small relative to the photon energy, ω, used here and are therefore neglected in practice. Note that in the case of a resonance, $\Delta E_{ai}(t) = 0$ and so the form of $\Omega_{ia}^{\pm}(t)$ is further simplified.

$\gamma_g(t) = 2\pi|\mu_{gi}|^2|\mathscr{E}_0(t)|^2$ is the photoionisation width of the state $|g\rangle$ that ionises it to the state $|i\rangle$, where μ_{gi} is the dipole transition element for the bound-continuum transition $|g\rangle \rightarrow |i\rangle$. $\gamma_i(t) = 2\pi|\mu_{if}|^2|\mathscr{E}_0(t)|^2$ is the photoionisation width of the state $|i\rangle$ that ionises it to the state $|f\rangle$, where μ_{if} is the dipole transition element for the bound-continuum transition $|i\rangle \rightarrow |f\rangle$. $\Gamma_a = 2\pi|V_{af}|^2$ is the decay width of the state $|a\rangle$ to the Fano continuum states $|f\rangle$, where V_{af} is the coupling of the AIS to the second continuum. q_a is the q-Fano parameter of the AIS [12]:

$$q_a = \frac{\mu_{ia}}{\pi(\mu_{if}V_{af})_{E_a}}.$$

For all of the above quantities, Γ_a and q_a are the only time-independent quantities. Note that the equation for the A^{2+} population, is not needed as we may use the conservation law for the populations, i.e. the sum of the populations is normalised to one as shown in Eqn. (1d). The electric field used here is a sinusoidal laser pulse, $E(t) = \mathscr{E}_0(t)cos(\omega t)$, with the time dependent envelope:

$$\mathscr{E}_0(t) = \mathscr{E}_0\sin^2(\Omega t), \quad (3)$$

where $\Omega = \omega/2n$ is the envelope frequency and n is the number of cycles per pulse. The pulse used for the rate equations in the present work is a Fourier transform limited (FTL) pulse, which is an approximation of an FEL pulse as the bandwidth due to the stochasticity of an FEL pulse is not considered.

The ionisation dynamics of the system are governed by these dynamical parameters, which need to be determined beforehand in order to solve this set of equations. Note that in the present study, we have not included further transitions from the AIS to higher continuum states as this is only expected to be probable at very high intensities outside of the range used here. A further application of these equations has been relegated to appendix A as it is of interest, but not in the main focus of this work. Other forms of the electric field can be used and in the present manuscript, results have been obtained using a square pulse in order to compare results with those obtained using analytical equations, which assume a constant field and have been derived below.

2.2. Analytical solutions for the square pulse case

In order to solve this system analytically, we assume a constant electric field such that $\mathscr{E}_0(t) = \mathscr{E}_0$ is time independent. In this case, all coefficients that include the quantities in Eqns. (1) become time-independent and as such, they are amenable to analytical solutions. Furthermore, we can model a square pulse by assuming that after the pulse duration, τ_P, none of the photon induced dynamics occur and we are left with only the time-independent decay width of the AIS. This decay will remove all of the population of the AIS and transfer it to the doubly ionised state $|f\rangle$. Thus, the states $|g\rangle$ and $|i\rangle$ remain constant after τ_P so that $\sigma_{gg}(t \rightarrow \infty) = \sigma_{gg}(\tau_P)$ and $\sigma_{ii}(t \rightarrow \infty) = \sigma_{ii}(\tau_P)$, while $\sigma_{aa}(t \rightarrow \infty) \rightarrow 0$ and $\sigma_{ff}(t \rightarrow \infty) \rightarrow \sigma_{ff}(\tau_P) + \sigma_{aa}(\tau_P)$.

It is then possible to rewrite Eqns. (1) using our knowledge of the initial conditions, i.e. $\sigma_{gg}(0) = 1$ and $\sigma_{ii}(0) = \sigma_{aa}(0) = \sigma_{ff}(0) = 0$, and by taking the Laplace transform [14], which leads to:

$$s\tilde{\sigma}_{gg}(s) = \frac{1}{s+\gamma_g}, \quad (4a)$$

$$s\tilde{\sigma}_{ii}(s) = A_i\sigma_{ii}(s) + \Omega_{ia}^{+}\sigma_{aa}(s) + \frac{\gamma_g}{s+\gamma_g}, \quad (4b)$$

$$s\tilde{\sigma}_{aa}(s) = \Omega_{ia}^{+}\sigma_{ii}(s) + A_a\sigma_{aa}(s). \quad (4c)$$

where

$$A_i = -\left(\gamma_i + \Omega_{ia}^{-} + \frac{|\Omega_0|^2}{q_a}\frac{\Delta E_{ai}}{\Delta E_{ai}^2+[(\gamma_i+\Gamma_a)/2]^2}\right),$$

$$A_a = -\left(\Gamma_a + \Omega_{ia}^{-} + \frac{|\Omega_0|^2}{q_a}\frac{\Delta E_{ai}}{\Delta E_{ai}^2+[(\gamma_i+\Gamma_a)/2]^2}\right).$$

The inverse Laplace transform can be performed on Eqn. (4a), or Eqn. (1a) can also be integrated easily to give

$$\sigma_{gg}(t) = e^{-\gamma_g t}, \quad (5)$$

whereas to obtain analytical solutions for Eqns. (4b) and (4c) we need to solve two equations with two unknowns. Once this is done we use the inverse Laplace transform to

the time domain to obtain the equations in time for $\sigma_{ii}(t)$ and $\sigma_{aa}(t)$:

$$\sigma_{ii}(t) = Qe^{-\gamma_g t} + Re^{\lambda_1 t} + Te^{\lambda_2 t} \tag{6a}$$

$$\sigma_{aa}(t) = Ke^{-\gamma_g t} + Le^{\lambda_1 t} + Me^{\lambda_2 t}, \tag{6b}$$

where

$$\lambda_1 = \frac{(A_i + A_a) + \sqrt{(A_i - A_a)^2 + (2\Omega_{ia}^+)^2}}{2},$$

$$\lambda_2 = \frac{(A_i + A_a) - \sqrt{(A_i - A_a)^2 + (2\Omega_{ia}^+)^2}}{2},$$

$$T = \frac{\gamma_g(1 - A_a)}{(\lambda_2 - \lambda_1)(\lambda_2 + \gamma_g)},$$

$$R = \frac{\gamma_g - (\lambda_2 + \gamma_g)T}{\lambda_1 + \gamma_g}, \qquad Q = -(R + T),$$

$$M = -\frac{\gamma_g \Omega_{ia}^+}{(\lambda_2 - \lambda_1)(\lambda_2 + \gamma_g)}, \qquad L = \frac{\lambda_2 + \gamma_g}{\lambda_1 + \gamma_g} M,$$

$$K = -(L + M).$$

2.3. Field fluctuations

It is also possible to add a term to Eqns. (1), which allows us to model the stochastic properties of the field in some way. The term is described in [6, 8, 15] and is shown here as the addition of the term γ_l in the following equations:

$$\langle \dot{\sigma}_{gg}(t) \rangle = -\gamma_g \langle \sigma_{gg} \rangle, \tag{8a}$$

$$\langle \dot{\sigma}_{ii}(t) \rangle = \gamma_g \langle \sigma_{gg} \rangle - \left(\gamma_i + \Omega_{ia}^- + \frac{|\Omega_0|^2}{q_a} \frac{\Delta E_{ai}}{\Delta E_{ai}^2 + [(\gamma_i + \Gamma_a + \gamma_l)/2]^2} \right) \langle \sigma_{ii} \rangle + \Omega_{ia}^+ \langle \sigma_{aa} \rangle, \tag{8b}$$

$$\langle \dot{\sigma}_{aa}(t) \rangle = \Omega_{ia}^+ \langle \sigma_{ii} \rangle - \left(\Gamma_a + \Omega_{ia}^- + \frac{|\Omega_0|^2}{q_a} \frac{\Delta E_{ai}}{\Delta E_{ai}^2 + [(\gamma_i + \Gamma_a + \gamma_l)/2]^2} \right) \langle \sigma_{aa} \rangle, \tag{8c}$$

$$\langle \sigma_{ff}(t) \rangle = 1 - \langle \sigma_{gg} \rangle - \langle \sigma_{ii} \rangle - \langle \sigma_{aa} \rangle, \tag{8d}$$

where

$$\Omega_{ia}^{\pm} = \frac{|\Omega_0|^2}{2} \left(\frac{(\gamma_i + \Gamma_a + \gamma_l)/2}{\Delta E_{ai}^2 + [(\gamma_i + \Gamma_a + \gamma_l)/2]^2} \right) \left(1 \pm \frac{1}{q_a^2} \right) \tag{9}$$

and

$$\gamma_l = \gamma_L \frac{\beta^2}{\Delta E_{ai}^2 + \beta^2} \tag{10}$$

which is introduced into the TDDM equation for the coherence evolution and allows us to model an added bandwidth due to phase fluctuations in the field. The frequency of the field fluctuates over a time scale $1/\beta$ and γ_L represents the field's bandwidth. β is the cut-off and has been set so that $\beta = \gamma_L$ in our calculations. Note that it is only possible to decorrelate the populations of the states when the fluctuations in the equations, i.e. Γ_a, γ_i, Ω_{ia} etc. are much slower than the fluctuations of the field due to the term γ_L.

3. Results

For the purpose of this paper, we have solved for the populations of the neon atomic states Ne($1s^2 2s^2 2p^6$; ^1S), Ne^+($1s^2 2s^2 2p^5$; ^2P), Ne^+($1s^2 2s^2 2p^4 6l$; ^1D), such that $l = s$ or d, and Ne^{2+}($1s^2 2s^2 2p^4$; ^3P) using each of the methods described above and with the following parameter values, in atomic units: $E_g = -2.299$, $E_i = -1.5054$, $E_a = 0.025247$, $E_f = 0.0$, $\mu_{gi} = 0.3477$, $\mu_{if} = 0.566$, $\mu_{ia} = 0.01731$, $\Gamma_a = 1.87 \times 10^{-4}$ and $q_a = 3.37$. As previously mentioned, these values were all determined from empirical results beforehand [16][1].

When reference is made to the 'resonant' and 'non-resonant' case, we refer to the use of a resonant photon energy, 41.65 eV, and a non-resonant photon energy, 41.3 eV, respectively. Of course, the choice of non-resonant photon energy is less strict than that of the resonant and the values for these energies will depend on the system and dynamics one wishes to model.

First, we begin by testing the applicability of the rate equations, i.e. Eqns. (1). The applicability of the rate equations for a system, as described in Fig. 1, has been tested by comparing the results of the rate equation approach to those of a TDDM approach [6] for the neon atomic system. The population of Ne^+ versus field intensity has been plotted separately in Figs. 2 and 3 for both the non-resonant and resonant case respectively. These results were obtained using a square pulse shape. It is clear that the results are in agreement when there is no strong resonance present, as shown in Fig. 2. However, when a strong resonance is present, as in Fig. 3, the results differ, particularly for longer field durations.

The applicability of the rate equations has also been tested for a sinusoidal pulse as described by Eqn. (3). The population of Ne^+ versus field intensity for such a pulse has been plotted separately in Figs. 4 and 5 for both

[1] *National Institute of Standards and Technology (NIST). http://www.nist.gov/index.html*

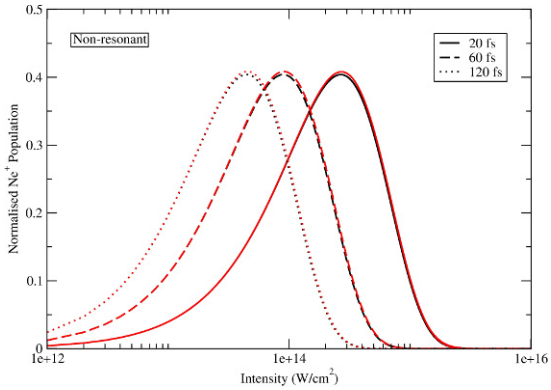

Figure 2. Population of Ne^+ after a constant field of 20 (full), 60 (dashed) and 120 (dotted) fs and using the TDDM (red) and rate (black) equation methods versus the intensity of the field. A non-resonant photon energy ($\omega = 41.3$ eV) was used. For the non-resonant case the position of the peak of the curve is dependent on the product of $I\tau_P$. The results obtained from both sets of equations coincide. The peaks of the Ne^+ populations occur at a value of approximately $I\tau_P = 6$ au.

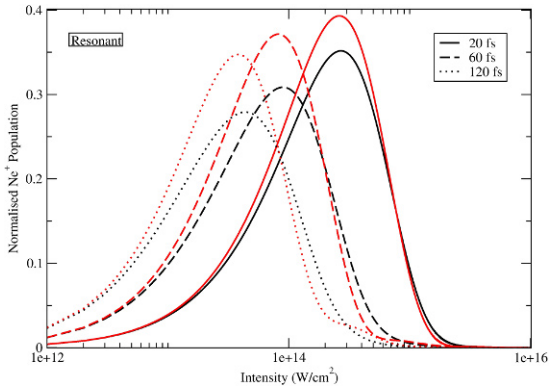

Figure 3. Population of Ne^+ after a constant field of 20 (full), 60 (dashed) and 120 (dotted) fs and using the TDDM (red) and rate (black) equation methods versus the intensity of the field. A resonant photon energy ($\omega = 41.65$ eV) was used. When using a resonant photon energy, the position of the peak is no longer linearly dependent on the product of $I\tau_P$.

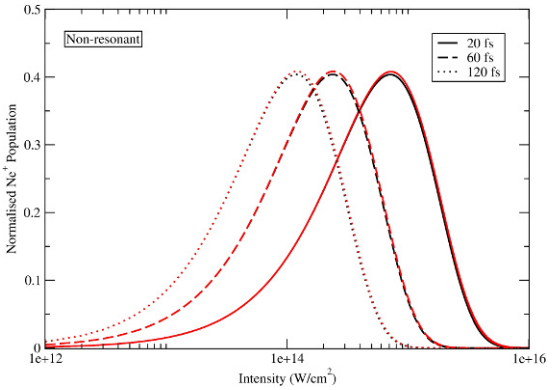

Figure 4. Population of Ne^+ after a 20 (full), 60 (dashed) and 120 (dotted) fs sinusoidal pulse and using the TDDM (red) and rate (black) equation methods versus the intensity of the pulse. A non-resonant photon energy ($\omega = 41.3$ eV) was used. For the non-resonant case the position of the peak of the curve is dependent on the product of $I\tau_P$. The results obtained from both sets of equations coincide. The peaks of the Ne^+ populations occur at a value of approximately $I\tau_P = 17$ au.

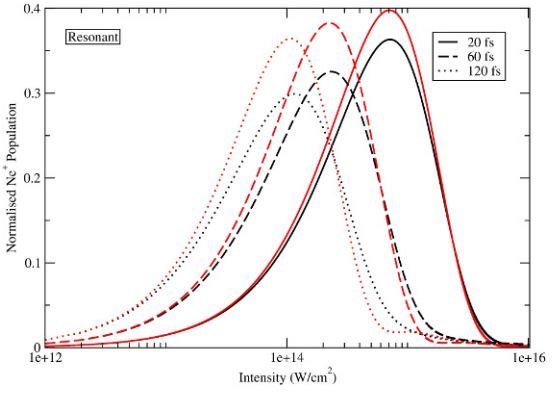

Figure 5. Population of Ne^+ after a 20 (full), 60 (dashed) and 120 (dotted) fs sinusoidal pulse and using the TDDM (red) and rate (black) equation methods versus the intensity of the pulse. A resonant photon energy ($\omega = 41.65$ eV) was used. When using a resonant photon energy, the position of the peak is no longer linearly dependent on the product of $I\tau_P$.

the non-resonant and resonant case respectively. Again, large differences in the results only appear when a strong resonance is involved.

Although the shapes of the curves are similar, the relative amplitudes of the populations are in disagreement in the resonant case. It appears that the rate equation method emphasises the effects of the resonance when compared to the TDDM method as the Ne^+ state is less populated in the rate equation results.

Also note that, in each of these figures, for both the resonant and non-resonant cases, each peak of the Ne^+ population curve occurs at the same value of $I\tau_P$, i.e. the product of the intensity and field duration, when using the rate equation method. However, when using the TDDM method, although the same is true for the non-resonant case, in the resonant case there is a slight deviation from this relationship that increases as the duration of the field increases as shown in Figs. 3 and 5. This shows the presence of non-linear effects due to the field when the res-

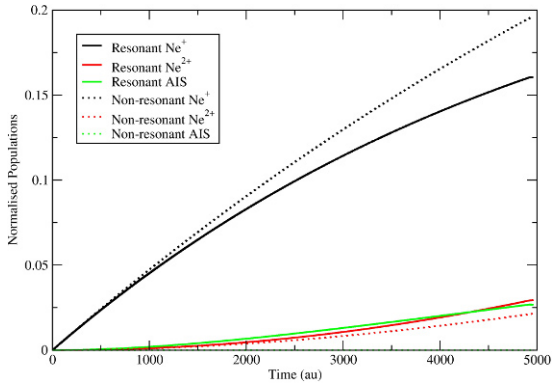

Figure 6. Populations of the ion species and AIS versus time for a field intensity of 1.0×10^{13} W/cm^2 and a period of up to 120 fs. The non-resonant AIS population is difficult to see since it maintains a zero value.

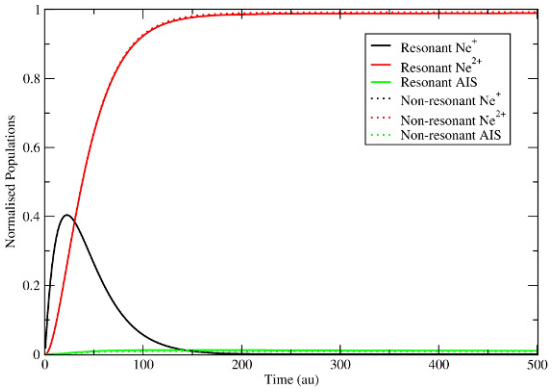

Figure 7. Populations of the ion species and AIS versus time for a field intensity of 1.0×10^{16} W/cm^2 and up to 12 fs. The Ne^{2+} population tends to 1 and the other populations vanish beyond this time.

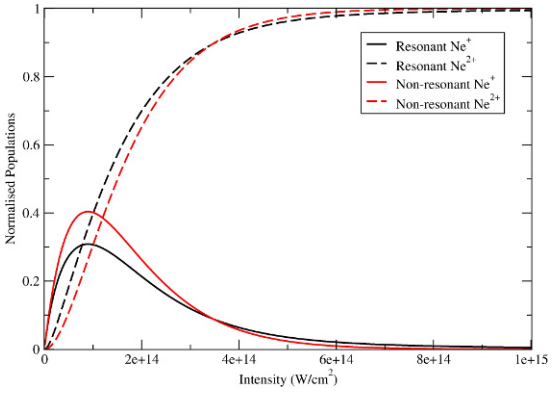

Figure 8. Population of Ne^+ (solid lines) and Ne^{2+} (dashed lines) after a constant field of 60 fs versus intensity of the field. The resonant case is shown in black and the non-resonant case in red.

onance with the AIS occurs, which are on the order of $(I\tau_P)^2$.

This has implications for the use of the rate equations when applying them to a system that includes a resonance with an AIS. The rate equation method does not capture the dynamical processes involved quite as well as the TDDM method does. An explanation is necessary for the discrepancy seen between the results of these two methods. As was said above, the derivation of the rate equations involves the adiabatic elimination of the TDDM coherence equations [6]. In many cases, the adiabatic elimination of the coherences that include continuum states approach a steady state quickly [7]. However, the coherences between bound states do not necessarily do so. In order to obtain the rate equations, one must eliminate all of the coherences, including those between the bound states, and this can lead to the discrepancies seen here. Of course, this will only be clear when the coherence between the bound states is large, as is the case when a resonant photon energy is used.

Next, we give a brief description of the time development of the populations as given by the rate and analytical equations. From this point onwards, all results are obtained using a square pulse shape. Note that the rate equation and analytical equation results are not both plotted in the figures that follow. This is simply due to the fact that they agree to an extent such that one curve would be hidden by the other.

The time development of the populations gives an insight into the dynamics of the system as the field causes the transition and ionisation processes. The dynamics are highly dependent on the field parameters such as intensity, photon energy and duration. In order to show this, Fig. 6 depicts the populations of the Ne^+, Ne^{2+} and AIS states as a function of time with a constant field intensity of 1.0×10^{13} W/cm^2. In this figure, the effects on the populations when using a resonant photon energy can be seen.

At higher intensities the effects of a strong resonance are less noticeable. This is shown in Fig. 7, which depicts the time development of the populations, but with a much higher intensity of 1.0×10^{16} W/cm^2. The effects are lessened by the fact that the effective Rabi oscillation between the Ne^+ and AIS states is much faster when the intensity is higher, since the effective Rabi oscillation term is proportional to the intensity of the field. At high intensities, the AIS does not decay to the second continuum as easily because the effective Rabi oscillation is a much faster process when compared to this decay. In this example with neon, this decay width is approximately 130 fs, as

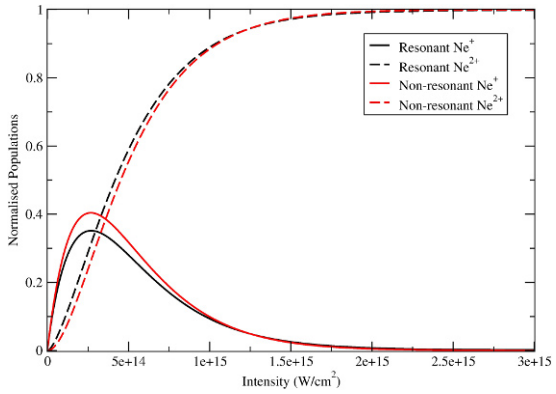

Figure 9. Populations of Ne^+ (solid lines) and Ne^{2+} (dashed lines), after a constant field of 20 fs, versus intensity of the field.

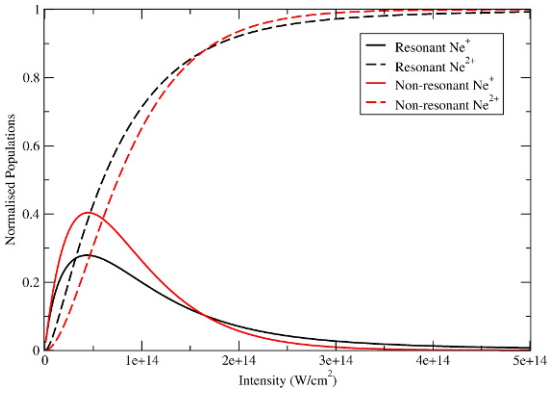

Figure 10. Populations of Ne^+ (solid lines) and Ne^{2+} (dashed lines), after a constant field of 120 fs, versus intensity of the field.

determined from the linewidth of 5.1 ± 0.2 meV FWHM obtained by Covington *et al.* [16].

Next, we show results for the variation of the populations with intensity of the external field. The population of the Ne^{2+} state in the figures that follow is actually the sum of the populations of the states $|f\rangle$ and $|a\rangle$ since it is assumed that, after the field is switched off, the AIS population decays to the Ne^{2+} state, as described in Section 2.2.

In Fig. 8, the population of Ne^+ and Ne^{2+}, after a 60 fs constant field, have been plotted against the field intensity. The effect of the Ne^+ - AIS resonance on the Ne^+ and Ne^{2+} yields is clear. In the resonant case there is an extra channel of ionisation when compared to the non-resonant case, which leads to an enhancement of the Ne^{2+} yield. The Ne^+ yield is also lowered since there are two highly probable absorption channels by which this state can be depopulated.

However, at field intensities greater than approximately 4×10^{14} W/cm^2, the yields of the two ion states do not follow this pattern. This is due to the fact that the effective Rabi oscillation occurring between the bound states is proportional to the field intensity and so, at some point, the effects of the effective Rabi oscillation will be larger than those of the AIS decay width, which decays to the second continuum. Thus, the likelihood of ionisation via the AIS state is decreased.

The Ne^+ and Ne^{2+} yields have also been plotted in Fig. 9 and 10 when using a 20 fs and 120 fs field duration respectively. These figures show both the resonant case and non-resonant case results. The same pattern is seen for all field durations. However, the Ne^{2+} yield saturates more easily when using a longer pulse, as would be expected due to the larger photon exposure. Also, as the duration of the field increases, the effects of the resonance

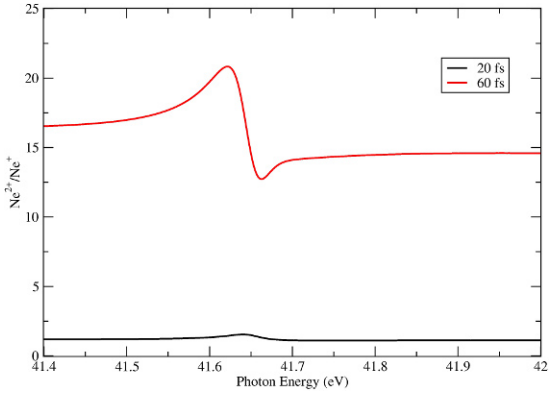

Figure 11. Ion yield ratio after a constant field of 20 fs (black line) and 60 fs (red line) versus photon energy. These results were obtained using a field intensity of 4×10^{14} W/cm^2.

are more noticeable. Note that the ranges of the x-axes on Figs. 8, 9 and 10 are all different.

Finally, we show results for the ratio of the final ion populations for different photon energies. These results give us another way to show the effects of the resonance on the Ne^+ and Ne^{2+} populations. A peak in this graph indicates the presence of a resonance near the second ionisation threshold. Fig. 11 shows this ratio when using a 20 fs and a 60 fs field duration. The effects can clearly be seen around 41.65 eV. This is in agreement with the experimentally determined value for the resonance energy as given by Covington *et al.* [16].

When using a 120 fs pulse duration, an interesting feature appears in the ion yield ratio. This is illustrated in Fig. 12. As the duration of the field is increased, the resolution of the generated ion yield ratio also increases. At

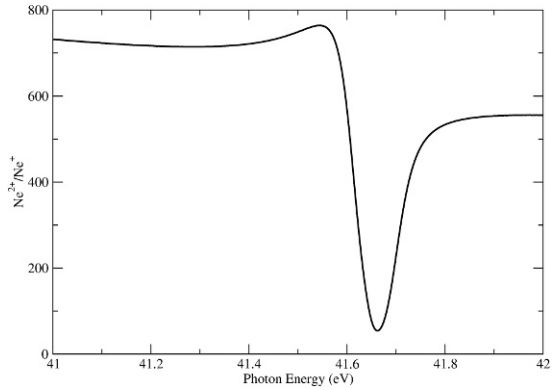

Figure 12. Ion yield ratio after a constant field of 120 fs versus photon energy. These results were obtained using a field intensity of 4×10^{14} W/cm^2.

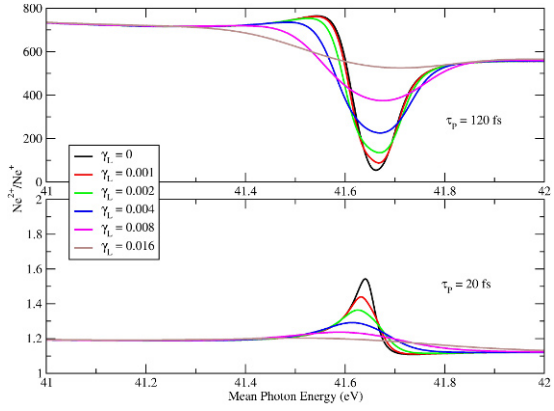

Figure 13. Ion yield ratio after a constant field of 20 fs ($1/\tau_P = 1.210 \times 10^{-3}$ au, lower figure) and 120 fs ($1/\tau_P = 2.016 \times 10^{-4}$ au, upper figure) versus the mean photon energy. The different curves show the ion yield ratio that was obtained with various added bandwidths from 0 to 0.016 au. The AIS decay rate is $\Gamma_a = 1.87 \times 10^{-4}$ au. These results were obtained using a field intensity of 4×10^{14} W/cm^2.

this combination of field duration and intensity, there is a minimum at the resonance energy.

In Fig. 13 the ion yield ratios have been plotted with different values of γ_L in order to test the effects of the added bandwidth on the ion yields. It is clear from the figure that a broadening of the bandwidth results in a broadening of the ion yield ratio. Particularly, when $\gamma_L = 0.016$, the peaks in the ratio are greatly diminished.

4. Conclusions

The applicability of the rate equations used here were tested against the more robust TDDM equations and the results show that the rate equations do not fully follow the dynamics of the system when a resonant photon energy is used. However, the results agree when a non-resonant photon energy is used. In other words, the rate equations are a good approximation when no strong resonances are involved in the dynamics of the system under study.

For the square pulse case, the analytical equations were also used to obtain results for the neon atom with various field conditions including intensity, photon energy and duration. These results were in agreement with those of the rate equations. Thus, these analytical equations can be used to estimate the populations of ion species for a three-level noble gas atom. However, when one includes a resonance with an AIS, one must be careful when making claims about the populations and consider the effects of the resonance on the validity of the results.

Finally, an attempt at modelling the stochastic nature of the field was made by adding an effective bandwidth to the equations. The results showed that the added bandwidth diminishes and broadens the ion yield ratio's peak.

Acknowledgements

D.P.W.M. and L.A.A.N. would like to acknowledge the support of the COST action CM0702. D.P.W.M. is supported by the Irish Research Council (IRC) through the EMBARK initiative. L.A.A.N. is supported by the Science Foundation Ireland (SFI) Stokes Lectureship Program. K.N.R.T. is supported by the DCU Summer Internship Program.

Appendix A

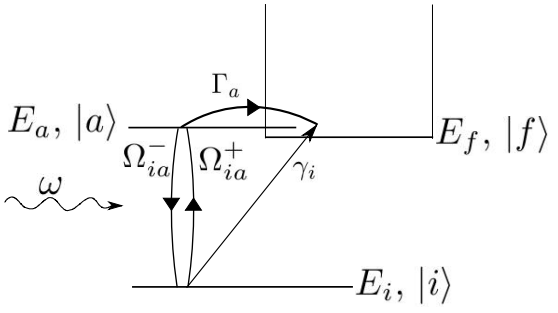

Figure 14. The states involved in the transitions for a two level noble gas system with an AIS. The terms in this figure are described in sections 2 and 2.1.

Eqns. (1) allow the calculation of the populations of a three level system with an AIS that interacts with an intense UV/X-ray field. However, note that it is also pos-

sible to obtain a set of equations for a two level system under similar conditions, as shown in Fig. 14, by simply setting the term $\sigma_{gg}(t) = 0$ for all t and changing the initial conditions so that $\sigma_{ii}(0) = 1$ and $\sigma_{aa}(0) = \sigma_{ff}(0) = 0$. This leads to the following set of equations:

$$\dot{\sigma}_{ii}(t) = -\left(\gamma_i + \Omega_{ia}^{-} + \frac{|\Omega_0(t)|^2}{q_a}\frac{\Delta E_{ai}}{\Delta E_{ai}^2 + [(\gamma_i + \Gamma_a)/2]^2}\right)\sigma_{ii} + \Omega_{ia}^{+}\sigma_{aa}, \tag{A1a}$$

$$\dot{\sigma}_{aa}(t) = \Omega_{ia}^{+}\sigma_{ii} - \left(\Gamma_a + \Omega_{ia}^{-} + \frac{|\Omega_0(t)|^2}{q_a}\frac{\Delta E_{ai}}{\Delta E_{ai}^2 + [(\gamma_i + \Gamma_a)/2]^2}\right)\sigma_{aa}, \tag{A1b}$$

$$\sigma_{ff}(t) = 1 - \sigma_{ii}(t) - \sigma_{aa}(t), \tag{A1c}$$

which can also be adapted to be solved analytically or to include stochastic properties as described in the main text.

References

[1] W. Ackermann et al., Nat. Photonics 1, 336 (2007)

[2] V. Richardson et al., J. Phys. B: At. Mol. Phys. 45, 085601 (2012)

[3] L. Young et al., Nature (London) 466, 56 (2010)

[4] L. A. A. Nikolopoulos, P. Lambropoulos, J. Phys. B: At. Mol. Phys. 40, 1347 (2007)

[5] M. Meyer et al., Phys. Rev. A 74, 011401 (2006)

[6] D. P. W. Middleton, L. A. A. Nikolopoulos, J. Mod. Opti. 59, 1650 (2012)

[7] L. A. A. Nikolopoulos, T. J. Kelly, J. T. Costello, Phys. Rev. A 84, 063419 (2011)

[8] B.-N. Dai, P. Lambropoulos, Phys. Rev. A 34, 3954 (1986)

[9] P. Lambropoulos, P. Zoller, Phys. Rev. A 24, 379 (1981)

[10] K. Blum, Density matrix theory and its applications (Plenum Press, 1981)

[11] M. Martins, M. Wellhöfer, A. A. Sorokin, M. Richter, K. Tiedtke, W. Wurth, Phys. Rev. A 80, 023411 (2009)

[12] U. Fano, Phys. Rev. 124, 1866 (1961)

[13] S. Stenholm, Foundations of Laser Spectroscopy (John Wiley and Sons, 1984)

[14] R. Bellman, R. S. Roth, Laplace Transforms (Singapore, World Scientific, 1984)

[15] P. Agostini, A. T. Georges, S. E. Wheatley, P. Lambropoulos, M. D. Levenson, J. Phys. B: At. Mol. Phys. 11, 1733 (1978)

[16] A. M. Covington et al., Phys. Rev. A 66, 062710 (2002)